CrossMark

RESEARCH ARTICLE

Reducing Spatial Heterogeneity of MALDI Samples with Marangoni Flows During Sample Preparation

Yin-Hung Lai,[1] Yi-Hong Cai,[1] Hsun Lee,[1] Yu-Meng Ou,[1,2] Chih-Hao Hsiao,[1] Chien-Wei Tsao,[1,3] Huan-Tsung Chang,[2] Yi-Sheng Wang[1]

[1]Genomics Research Center, Academia Sinica, Taipei, 115, Taiwan, Republic of China
[2]Chemistry Department, National Taiwan University, Taipei, 106, Taiwan, Republic of China
[3]Department of Chemical Engineering and Biotechnology, National Taipei University of Technology, Taipei, 106, Taiwan, Republic of China
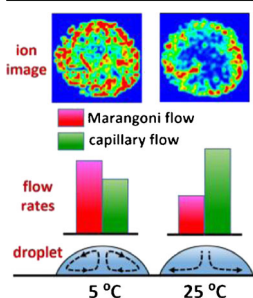
Abstract. This work demonstrates a method to prepare homogeneous distributions of analytes to improve data reproducibility in matrix-assisted laser desorption/ionization (MALDI) mass spectrometry (MS). Natural-air drying processes normally result in unwanted heterogeneous spatial distributions of analytes in MALDI crystals and make quantitative analysis difficult. This study demonstrates that inducing Marangoni flows within drying droplets can significantly reduce the heterogeneity problem. The Marangoni flows are accelerated by changing substrate temperatures to create temperature gradients across droplets. Such hydrodynamic flows are analyzed semi-empirically. Using imaging mass spectrometry, changes of heterogeneity of molecules with the change of substrate temperature during drying processes are demonstrated. The observed heterogeneities of the biomolecules reduce as predicted Marangoni velocities increase. In comparison to conventional methods, drying droplets on a 5 °C substrate while keeping the surroundings at ambient conditions typically reduces the heterogeneity of biomolecular ions by 65%–80%. The observation suggests that decreasing substrate temperature during droplet drying processes is a simple and effective means to reduce analyte heterogeneity for quantitative applications.

Keywords: MALDI, Heterogeneity, Spatial distribution, Marangoni flow, Hydrodynamic flow, Sample preparation, Substrate temperature

Introduction

Matrix-assisted laser desorption/ionization (MALDI) is an indispensable technique for mass analyses of analytes prepared on surfaces [1, 2]. MALDI is highly efficient for ionizing biomolecules [3–5]. It relies on co-crystallizations of trace analytes with matrix compounds, but the typical sample morphology and spatial distribution of analytes are highly irregular. The heterogeneous analyte distributions result in poor data reproducibility [2, 6, 7] and make quantification analysis with MALDI mass spectrometry (MS) difficult [8]. The reasons for a heterogeneous spatial distribution of molecules, or

heterogeneity defined hereafter, may involve multiple factors during droplet drying processes, such as physical properties of solutes [9], viscosity of solutions [10], and hydrodynamic flows inside droplets [11].

Natural-air drying processes typically result in heterogeneous spatial distributions of analytes after drying. The analyte distributions in MALDI samples have been studied with imaging MS [12–16]. Although some MALDI samples form uniform crystal morphologies, they show high ion yields only at peripheral regions [17, 18]. The irregular ion distribution and abundant ion signal at sample periphery are known as the "sweet-spot" [7, 19–21] and "hidden coffee-ring" [11] effects, respectively. These heterogeneity problems make diagnosis of molecules with low ionization efficiency even more difficult, especially for carbohydrates [22–24]. Although fast evaporation [12], concentration adjustment [25], substrate manipulation [11], and electric-induced droplet circulation [26] can reduce heterogeneity, these methods are not generally

applicable and may reduce the ionization efficiency of analytes. Thus, a convenient and general method to reduce the sample heterogeneity is highly necessary.

The mechanistic details of pattern formation, especially those responsible for general macroscopic ring-stain formation, have been studied by Deegan et al. [17] and Hu et al. [27]. The results in those works suggest that internal outward capillary flows induced by solvent evaporation carry molecules toward the droplet's edge. Such outward capillary flows may responsible for the hidden coffee-ring effects in MALDI. Such outward capillary flows can be counterbalanced by recirculation flows, or Marangoni vortexes, induced by tangential gradients of surface tension at droplet's surface [28]. Although a reduction in the heterogeneity of abundent components by Marangoni flows can be visualized after drying [29], the spatial distribution of trace components, such as analytes in MALDI, is invisble and needs further analysis.

This work demonstrates a simple method to reduce the heterogeneity of MALDI samples for quantitative applications. The heterogeneity of analytes originally dissolved in matrix solutions is reduced by temperature-induced Marangoni flows during drying processes. The drying environment is controlled at ambient conditions of 1 atm and 25 ± 0.8 °C. The only adjusted parameter is the substrate temperature during drying processes. The competition between evaporation-driven outward caplillary flows and temperature-induced Marangoni flows is analyzed theoretically. Changes in heterogeneity of two model carbohydrates, isomaltotriose (IM3) and α-cyclodextrin (α-CD), and one protein, angiotensin I (ANG), are analyzed with MALDI imaging MS. The matrix compounds involved in this work include 2,4,6-trihydroxyacetophenone (THAP) and α-cyano-4-hydroxycinnamic acid (CHCA). These matrix compounds are used because they form homogeneous crystal morphologies after drying. The homogeneous morphologies minimize interference from uneven crystal structures to the spatial distribution of analytes in such samples. This is the first attempt experimentally to reduce the heterogeneity of MALDI samples by temperature-induced hydrodynamic flows during sample preparation. The results of imaging MS and quantitative region of interest (ROI) analyses indicate that decreasing substrate temperature during sample preparation reduces analyte heterogeneity. The method is simple and is expected to be effective for quantitative applications.

Experimental

All matrixes and analytes were purchased from Sigma (Sigma-Aldrich Co., St. Louis, MO, USA). Acetonitrile (ACN, Merck, Darmstadt, Germany) and deionized water (Milli-Q water purification system, Millipore, Billerica, MA, USA) were used to prepare the sample and matrix solutions. THAP and CHCA were dissolved in 50% and 90% ACN to a concentration of 0.1 M, respectively. Both aqueous sample solutions of IM3 and α-CD were prepared using deionized water to a concentration of

10^{-4} M for the case of THAP as the matrix. α-CD was prepared in 40% ACN to a concentration of 10^{-3} M when CHCA was used as matrix. The high concentration of α-CD in this case is due to its lower sensitivity with CHCA. ANG was dissolved in 50% ACN to a concentration of 10^{-5} M. Equal volumes of matrix and sample solutions were premixed, and 0.1 μL of the solution was deposited on MALDI substrate surface for drying. The morphologies of the dried samples were examined by an optical microscope (SZX16; Olympus, Tokyo, Japan) before conducting imaging MS analyses.

The drying process was performed in a 35 × 20 × 45 cm (W × D × H) acrylic drying chamber, as shown in Figure 1. The right-hand side of the chamber is a sliding door that is closed except for solution deposition or when crystallizations are completed. The drying chamber is purged by room-temperature nitrogen in a constant flow rate of 10 SCFM to a relative humidity of 20%–25%, as monitored by a hygrometer. A copper base block equipped with a programmed constant temperature water circulator (J-606; Jorfai Co., Hsinchu, Taiwan) is installed in the drying chamber to support stainless-steel MALDI sample plates. The copper base block is able to regulate the substrate temperature from 5 to 45 °C, with accuracy of ±0.1 °C. The precise temperature control ensures that the thermodynamic properties of the droplet can be applied to theoretical simulations. Sample solutions are deposited on the sample plate for drying. Before droplet deposition, the relative humidity within the chamber is carefully controlled to avoid water condensation on the sample and the substrate surface. A CCD camera outside the chamber monitors the evaporation processes. The obtained video files are used to estimate the evaporation rate.

The ambient and substrate temperatures are monitored with K-type thermocouples. The ambient temperature at approximately 1.0-mm above the substrate defines the ambient temperature. This temperature is the boundary temperature for
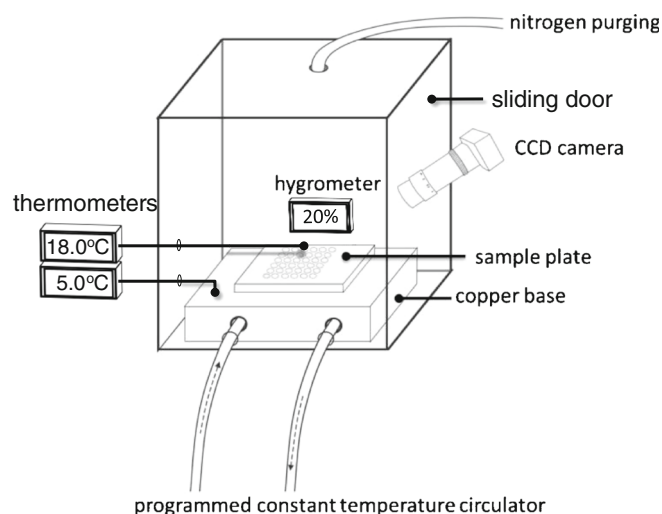

Fig. 1. The schematics of the acrylic drying chamber. The sliding door to the right of the drying chamber is always closed except for depositing sample droplets and when crystallizations are completed

simulations. The substrate temperatures (T_S) used include 5, 10, 15, 20, 25, 35, and 45 °C. In the cases of 5–15 °C, the sliding door is opened after the samples are completely dried, and the substrate is warmed up to room temperature before being removed from the drying chamber.

The imaging mass spectrometry analysis is conducted using a laboratory-made synchronized dual-polarity time-of-flight imaging mass spectrometer (DP-TOF IMS) that has been described previously [30]. A pulsed UV laser beam (349 nm, Explore One; Spectra-Physics Inc., Santa Clara, CA, USA) examines samples with a fluence of roughly 80 J/m^2. The laser beam is focused by a plano-convex lens to a circular spot with a diameter of 35 μm. The pitch of adjacent sampling spots is 40 μm. The spectrum of every spot is the average of five laser shots. The kinetic energy of ions is 20 keV, and the extraction delay is optimized for different samples.

Both mass spectrometric images and mass spectra are analyzed by using software developed in-house. The signal intensity is normalized for every image, and the relative intensity is displayed with different colors. For the numerical region-of-interest (ROI) analysis, every sample is divided laterally into five concentric layers with equal annular width, as shown in Section A of Supporting Information. The five ROIs from the center to the periphery are defined sequentially from ROI 1 to ROI 5. The relative signal intensity of ions in the ROI analysis contains three sets of data obtained under identical conditions. Relative standard deviations (RSD, in percentage) are used as the quantitative basis for the comparison of heterogeneity of samples. In every individual set of data, the interference of fine gaps within sample crystals is eliminated by removing sample spots if the signal-to-noise ratios of protonated as well as sodiated matrixes and analytes are below 3.

The average velocity of outward capillary flow induced by evaporation is derived from the fundamental formulas of evaporation flux proposed in literature [18, 31, 32]. In the present study, the formulas are extended to obtain the average evaporation rate based on the result of a semi-empirical analysis. A detailed discussion of the calculation is summarized in Section B of Supporting Information. Finite element modeling (FEM) for calculating the strength of Marangoni flow is performed using a commercial simulation software (COMSOL Multiphysics v5.0, COMSOL Inc., Stockholm, Sweden). The conservations of mass, momentum, and energy are considered simultaneously. The Marangoni boundary along the surface of the droplet is also applied to the simulation [28]. The predicted strength of Marangoni flow is obtained by a two-step correction process, including the correction for solvent constituent and an empirical scaling factor of 0.01 suggested by Hu et al. [33]. The final scaling factor is 0.0088. The interferences of analytes to the hydrodynamic flow are ignored due to their low abundances. Section C of Supporting Information describes the boundary conditions and thermodynamic properties for simulations.

Results and Discussion

Simulation of Hydrodynamic Flows in Drying Droplets

The theoretical analysis provides a thorough insight into the mechanistic detail of molecular flows under various conditions inside the drying chamber. Within this chamber, temperature gradients in droplets can be produced by changing T_S away from its surroundings. The simulation result shows that flow fields inside droplets change when temperature gradients within droplets change. Supplementary Figure S1 in the Electronic Supporting Information Section D shows predicted temperature gradients within a cross-section of a droplet when keeping the T_S at 5, 25, and 45 °C. Notably, the results represent the conditions at the instants the drying processes start. Since heat conduction is more efficient via the substrate than heat convection is through air, the average droplet temperature is near that of T_S. According to the prediction, the bottom of the droplet in every case has the identical temperature to T_S, and the temperature at the top of the droplet slightly shifts towards the surroundings. Keeping T_S at 5 °C, for example, results in a smooth increase of temperature from the bottom to the top of the droplet, in which the top is approximately 0.23 °C warmer than the bottom (5 °C). When keeping T_S at 45 °C, the temperature inside the droplets shows curved gradients, and the top of the droplet is approximately 0.24 °C cooler than the bottom (45 °C). When keeping T_S at 25 °C while the ambient temperature is at 24.4 °C (a representative observed condition), the droplet surface is ~0.01 °C cooler than the bottom.

The decrease in droplet mass is mainly due to the evaporation of solvent molecules near the boundary between liquid, substrate, and air [17, 27]. This boundary is known as the contact line of the droplets. In the present study, the boundary region of the droplet beyond 94% contact line radius defines the effective contact (E.C.) region. The fast evaporation of solvent molecules at the surface of this region induces outward capillary flows within the entire droplet [17, 32]. Since the speed of evaporation depends on temperature, the velocity of such outward capillary flows (V_C) also depends on temperature. According to the semi-empirical analysis under T_S of 5, 25, and 45 °C, the resultant average V_C of the entire droplet ($<V_C>$) are 5.17 × 10^{-7}, 4.70 × 10^{-6}, and 1.80 × 10^{-5} m/s, respectively. Therefore, slower outward capillary flows under lower T_S conditions are more easily overcome by other hydrodynamic flows.

The velocity of Marangoni flow (V_M) inside a droplet depends on the magnitude of the temperature gradient along the droplet surface [18, 28, 32]. Adjusting T_S away from ambient temperatures (either upward or downward) increases temperature gradients and V_M. Figure 2 shows magnitudes and directions of calculated V_M under the three T_S conditions used in Supplementary Figure S1. Under these conditions, the bottom and significant part of the subsurface layer of the droplets have slower V_M (i.e., dark areas in the figures) than the rest of the area, whereas the droplet surface has the fastest V_M.
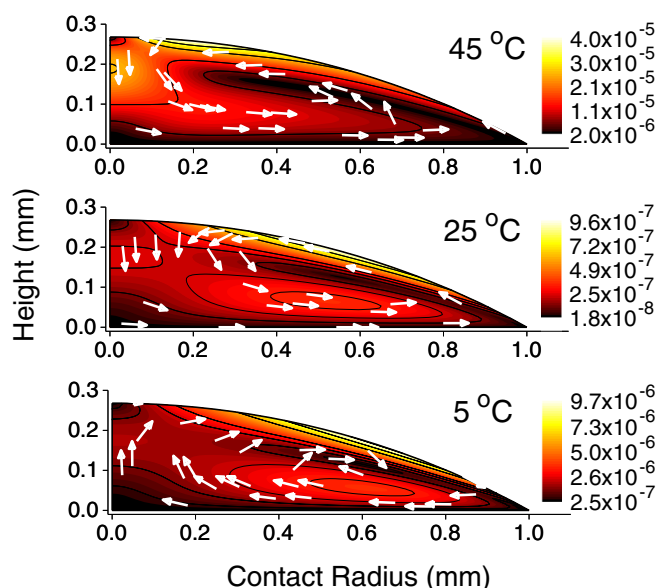
Fig. 2. The calculated velocity of Marangoni flow inside a drying droplet while keeping the substrate temperature at 5, 25, and 45 °C. The air above the droplet is kept at ambient temperature determined experimentally. The color represents the velocity of Marangoni flow, and the arrows represent the flow direction. The corresponding Marangoni velocity of the color is denoted to the right
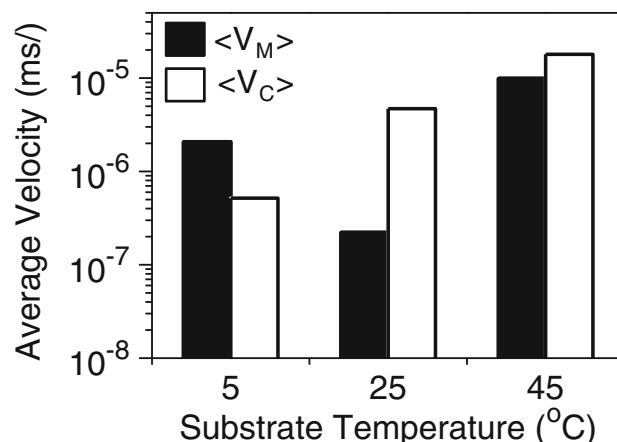

Fig. 3. Comparison of various average flow velocities of the entire droplet under different substrate temperatures. Black bar: average Marangoni flow; white bar: average capillary flow

Based on the results of the calculations, the direction of Marangoni vortex at any point inside the droplet is different. It is distinct from the evaporation-induced outward capillary flows that always pull molecules from the center to the periphery of the droplets [17]. As shown in Figure 2, the Marangoni vortex in the central area of the droplet is counterclockwise when the T_S is kept at 25 and 45 °C. Under these T_S conditions, the streamlines of Marangoni flow move from the center towards the E.C. region along the bottom of the droplet. Before entering the E.C region, the streamlines ascend along the droplet surface towards the upper part of the droplet and then return to the bottom. Such a flow field agrees with those reported in the literature [33–35]. When keeping T_S at 5 °C, on the other hand, the direction of streamlines of Marangoni flow reverse and become clockwise; they move from the region next to the E.C. region toward the droplet center along the bottom, then ascend to the top and return to the region next to the E.C. region along the droplet surface. These simulations suggest that a cold substrate provides superior Marangoni flows than a hot substrate for recirculation of molecules.

The final flow field within a droplet is the result of competition between the $<V_C>$ and the average V_M of the entire droplet ($<V_M>$). The result of this competition strongly affects the spatial distribution of molecules after drying. Figure 3 compares the $<V_C>$ and $<V_M>$ when T_S are 5, 25, and 45 °C. When keeping T_S at 25 °C, the $<V_M>$ is 2.22×10^{-7} m/s, which is only roughly 5% of that of $<V_C>$. Such a slow Marangoni flow is attributed to insignificant temperature gradient. In fact, within the E.C. region, the average velocity of Marangoni flows is more than 1800 times slower than that of the outward capillary

flows when T_S is 25 °C, as illustrated in Supplementary Figure S2, Section D, Supporting Information. The prediction suggests that outward capillary flows dominate the drying process when T_S only differs from its surroundings by ~0.6 °C. Thus, the Marangoni flow is negligible if no temperature change is applied to the substrate. This result explains reasonably the intense analyte signal present at the periphery of MALDI samples reported in the literature [11].

When T_S decreases, the $<V_M>$ increase whereas the $<V_C>$ decrease. Under $T_S = 5$ °C, the $<V_M>$ is 2.08×10^{-6} m/s, which is roughly nine times faster than that at 25 °C. This $<V_M>$ is roughly four times faster than the corresponding $<V_C>$ (Figure 3), suggesting that the Marangoni flows can overcome outward capillary flows under this condition. In the E.C. region, however, the average velocity of Marangoni flow is ~17 times slower than that of the outward capillary flow (Supplementary Figure S2). The result indicates that Marangoni vortexes dominate the drying process within the droplet when $T_S = 5$ °C, even though the outward capillary flow still dominates the E.C. region. Based on the prediction under this condition, the Marangoni flows can recirculate molecules within 85% contact line radius.

In contrast to the result obtained when T_S is 5 °C, increasing T_S from 25 to 45 °C increase the $<V_M>$ and $<V_C>$ simultaneously but with different magnitudes. Under $T_S = 45$ °C, the $<V_M>$ increases by approximately 45 times than that under 25 °C. However, the resultant $<V_M>$, 9.93×10^{-6} m/s, is still only 55% that of $<V_C>$ under the same condition (Figure 3). On the other hand, the average velocity of Marangoni flows in the E.C. region is 270 times slower than that of outward capillary flow in the same region (Supplementary Figure S2). This prediction suggests that under $T_S = 45$ °C, the reduction of heterogeneity of analytes should be less pronounced than that under $T_S = 5$ °C. Therefore, keeping T_S colder than its surroundings is expected to provide a better flow field in the droplet than warmer T_S for reducing heterogeneity of analytes.

Imaging Mass Spectrometry and Numerical Region of Interest Analysis

(a) *Imaging MS of analytes prepared with THAP*:

Mass spectrometry images are used for qualitative analysis of heterogeneity. The ion images of trace molecules co-crystalized with matrix compounds show apparent hidden coffee-ring effect when $T_S = 25$ °C. Figure 4 shows representative bright field and ion images of various analytes mixed with THAP and dried under six T_S conditions, namely 5, 10, 15, 20, 25, and 45 °C. The resultant sample areas are circular shaped with diameters of roughly 1.2–1.7 mm. The crystals prepared under lower T_S show more fine gaps than those under higher temperature. Because matrix crystallization starts from various locations within a droplet, it rapidly develops multiple crystal domains and gaps between domains presents. Such gaps are generally observed in MALDI samples and no clear evidence shows that they seriously affect the population of analytes.

The ion images show various kinds of heterogeneity. In the case of sodiated α-CD, a marked hidden coffee-ring effect occurs when T_S is kept under 25 and 20 °C. Under these conditions, the ion signal populates mainly within a narrow area at the periphery, and the central area shows much lower signal intensity. When decreasing T_S to 15 and 10 °C, the width of the peripheral area with intense sodiated α-CD signal considerably thickens, and the area of low signal intensity at the

center decreases. When decreasing T_S to 5 °C, the sodiated α-CD shows reasonably high signal intensity over the entire sample area, although the center is still slightly less intense than the rest of the area. Notably, increasing T_S to 45 °C improves ion population but the density of intense signal reduces dramatically. The ion population obtained under $T_S = 45$ °C does not improve data reproducibility.

The images of sodiated IM3 show a similar trend to those of sodiated α-CD, even though the reduction in heterogeneity with decreasing T_S for IM3 is less pronounced. An apparent hidden coffee ring of IM3 shows when preparing the sample under $T_S = 25$ °C. Reducing T_S to 20 °C improves the signal intensity at the central area, but the intensity at the periphery is still higher. When decreasing T_S to 15 and 10 °C, the population of high signal intensity spots slightly expands but some central areas exhibit low intensity. The best image of sodiated IM3 is obtained with $T_S = 5$ °C, in which neither a low intensity area nor an apparent aggregation of high intensity spots show. Increasing T_S from 25 to 45 °C reduces the density of high intensity spots of IM3 even while heterogeneity is reduced. This observation is similar to that of α-CD.

The reduction in heterogeneities with reducing T_S is also effective for ANG. The images of sodiated ANG are very similar to the protonated analogues. The reduction in heterogeneity is available even with minor changes to T_S. When keeping T_S at 25 °C, the center and partially the top area of ANG show low signal intensity. The low intensity area in this case is attributed to a thin matrix crystal, as shown in the corresponding bright field image; the matrix is an essential element of ionization reactions in MALDI [36–39]. By just decreasing T_S to 20 °C, the low intensity area diminishes. Further decreasing T_S increases the proportion of high intensity areas. The overall signal intensity is high when T_S is 10 and 5 °C, but gaps also become apparent. The ion images obtained with $T_S = 45$ °C results in similar result to those observed with $T_S = 10$ °C, except more low intensity areas show with 45 °C. Similar to α-CD and IM3, keeping T_S at 5 °C results in the largest high-intensity area for ANG.

(b) *Region of interest analysis*:

The numerical analysis of the concentric ROI provides useful information regarding the extent of hidden coffee-ring effect, as well as the general heterogeneity of analytes. Figure 5 shows the statistical results of ROI analyses of α-CD, IM3, and ANG prepared with THAP. Every data point contains three replicate measurements. For every sample and T_S, the average signal intensity of ROI is normalized. A general trend is that the variations of the data sequentially reduce as T_S decrease from 25 to 5 °C. The variation obtained with 45 °C is similar to that with 15 °C even though the trend of the ROI curve with 45 °C is different to other temperatures. These results agree nicely with the calculated results.

The most prominent evidence for the presence of hidden coffee rings is an ascending trend of signal intensity from inner to outer ROI. Such tends are found for α-CD and IM3 prepared under most T_S. Under $T_S = 25$ °C, the intensity at ROI 1 for α-CD and IM3 is 22% and 35% that of ROI 5, respectively.
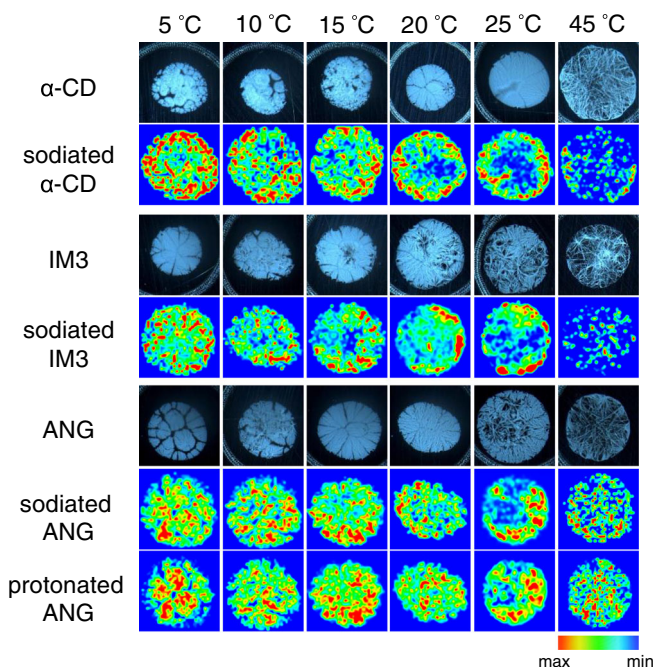

Fig. 4. Representative bright field and ion images of α-CD, IM3, and ANG in THAP under different substrate temperatures. From the left to right, the substrate temperature was 5, 10, 15, 20, 25, and 45 °C. The colored intensity scale bar for the ion images is shown at the bottom
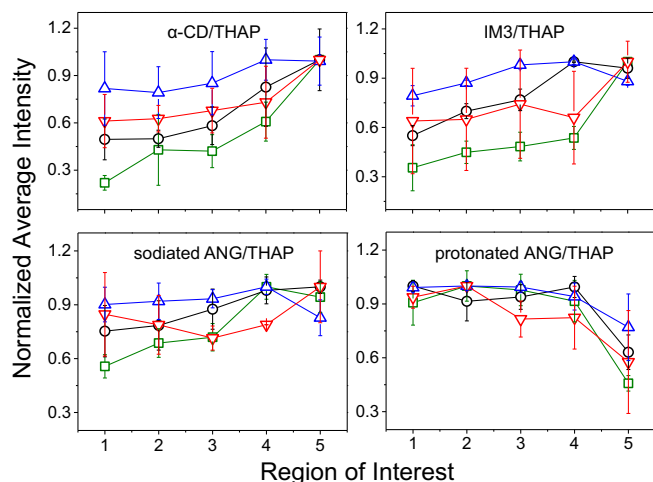
Fig. 5. The region of interest (ROI) analysis of MALDI images of α-CD, IM3, sodiated ANG, and protonated ANG prepared with THAP on four substrate temperatures; red, green, black, and blue data indicate samples prepared at substrate temperatures of 45, 25, 15, and 5 °C, respectively. The error bars are calculated based on three replicate tests
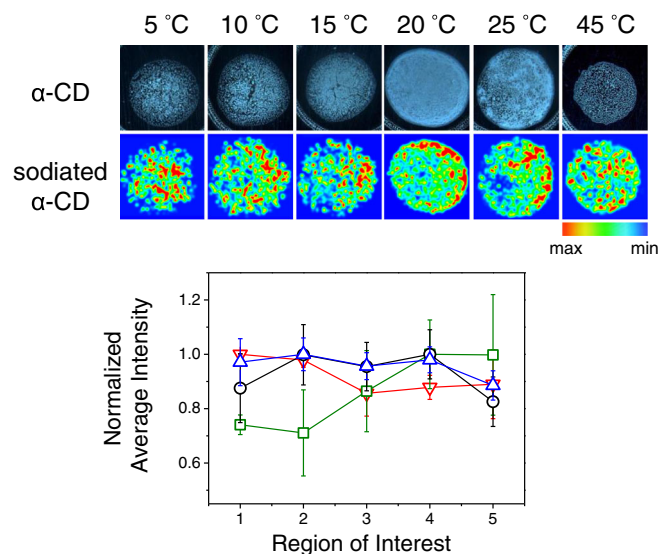

Fig. 6. Representative bright field (upper panel) and ion image (lower panel) of α-CD in CHCA at different substrate temperatures as well as the results of ROI analysis. The colored intensity scale bar for the ion signal is shown below the images. Red, green, black, and blue data of the ROI analysis indicate samples prepared at substrate temperatures of 45, 25, 15, and 5 °C, respectively. The error bars are calculated based on three replicate tests

Decreasing T_S to 15 and 5 °C increases the normalized intensity of ROI 1 to roughly 50% and 80%, respectively, and the slope of these curves decrease accordingly. Since smaller slopes imply less coffee-ring effect, the data suggests that preparing samples under $T_S = 5$ °C results in least hidden coffee-ring effects.

The result of ROI analysis of ANG is distinct from that of α-CD and IM3. The most significant difference is that the ascending trends of signal intensity from inner to outer ROI are less pronounced in the cases of sodiated ANG, and protonated ANG shows descending trends in all cases. Despite showing different trends to the carbohydrates, ANG still show less signal variations when decreasing T_S from 25 to 5 °C. For example, the signal variations for sodiated ANG are 44, 25, and 17% when keeping T_S at 25, 15, and 5 °C, respectively. For protonated ANG, these values become 54, 37, and 23%, respectively. The data curve of protonated and sodiated ANG obtained with $T_S = 45$ °C differs slightly from other temperatures, but the signal variation is similar to those at 15 °C. Therefore, keeping $T_S = 5$ °C is still the best condition. The statistical results indicate that a colder substrate is superior to a warmer substrate for decreasing heterogeneity of analytes in MALDI.

(c) *Validation with CHCA*:

Reductions in heterogeneity are also available when using CHCA as the matrix. Figure 6 shows representative bright field and ion images of α-CD prepared with CHCA, as well as the corresponding results of ROI analysis. The bright field images show that crystal morphologies are uniform at 20 and 15 °C. The thickness of samples becomes inhomogeneous and fine gaps between crystal domains show when T_S is 10 and 5 °C. The ion images show high signal intensities at peripheries for T_S of 25 and 20 °C. Decreasing T_S to 15, 10, and 5 °C moves the high intensity areas towards the center region. The

distribution of ion image under $T_S = 45$ °C is also better than that under 25 °C. The results of ROI analysis indicate that apparent hidden coffee rings present under $T_S = 25$ °C. Changing T_S efficiently removes the hidden coffee rings and reduces signal variation. The variations observed with 45, 25, 15, and 5 °C are 14, 29, 17, and 11%, respectively. Again, the best analyte distribution is obtained with $T_S = 5$ °C.

(d) *Reduction of heterogeneity with decreasing substrate temperature*:

A convenient index to quantify heterogeneity is the relative standard deviation (RSD) of the normalized average intensities of the five ROIs in every sample. In comparison to the ion images and statistical ROI analysis, RSD reveals quantitatively the general heterogeneity. Table 1 summarizes the RSD calculated using the results of ROI analyses in Figures 5 and 6. In every case, the RSD obtained with 25, 15, and 5 °C consistently reduces. For instance, the RSD of sodiated analytes reduces by roughly 40%–50% when decreasing T_S from 25 to 15 °C. Reducing the temperature from 15 to 5 °C further reduces the RSD of sodiated analytes by 42%–66%. In comparison to the result obtained with $T_S = 25$ °C, the reduction in RSD under $T_S = 5$ °C is very significant. In the cases of α-CD and IM3 prepared using THAP and CHCA, the RSD reduces by approximately 80%. The RSD of sodiated and protonated ANG reduces by 71% and 65%, respectively, with the same temperature change.

Except in the case of α-CD prepared using THAP, the RSD obtained with $T_S = 45$ °C in most cases is similar to that with 15 °C. Although a reduction in heterogeneity is achieved

Table 1. Relative Standard Deviation (in percentage) Among ROIs in Four Analyte/Matrix Systems Prepared at Four Substrate Temperatures

Substrate temperature (°C)	Relative standard deviation (%)				
	THAP				CHCA
	α-CD	IM3	ANG		α-CD
	$m + Na^+$	$m + Na^+$	$m + Na^+$	$m + H^+$	$m + Na^+$
5	11.05	9.42	6.77	9.28	4.44
15	32.88	23.46	12.68	17.00	7.68
25	54.87	44.66	23.68	26.27	15.25
45	21.73	20.59	12.94	19.49	6.99
Reduction of RSD from 25 to 5 °C	80%	79%	71%	65%	71%

by warming up the substrate during drying processes, increasing T_S by 20 °C above ambient conditions only offers the similar efficiency to that created by decreasing T_S by 10 °C. This result implies that the recirculation flow within droplets induced by a colder substrate is faster and more efficient than that induced by a warmer substrate with the same temperature difference.

Notably, Marangoni flows induced by the temperature gradient serve as an effective means to compete with other natural driving forces influencing the internal flow of analytes. Other driving forces include analyte adsorption [40], surfactant contamination [27], inadvertent solvent evaporation [41], and physicochemical properties of matrixes [28]. However, the reduction of heterogeneity with Marangoni flows for some matrixes are less efficient. An example is the samples prepared using 2,5-dihydroxybenzoic acid (DHB); this matrix forms apparent crystals at the periphery. Therefore, further improvement is necessary to enhance the hydrodynamic flows for overcoming the physicochemical phenomenon that lead to a lack of homogeneity within such matrix solutions. Additionally, a detailed study of changes in ion abundances by the hydrodynamic effects is planned for subsequent publications.

Conclusions

Marangoni flows within drying droplets induced by changes in the substrate temperature can redistribute analytes within MALDI samples. Such Marangoni flows reduce the heterogeneity of analytes after drying. The results of systematic imaging mass spectrometric and the region of interest analyses indicate that the most significant reduction in heterogeneity is obtained by decreasing substrate temperature to 5 °C. Under this condition, the relative standard deviation of the entire measure of the sample areas is reduced by 65%–80%. The result of theoretical simulations provide an insight into the mechanism of the change of hydrodynamic flows under different droplet drying conditions. By decreasing the substrate temperature to 5 °C while keeping its surroundings at ~25 °C during the drying process, the average Marangoni flow within droplets is four times faster than the outward capillary flows induced by solvent evaporation. This sample preparation method is convenient and generally effective. Such improvements in spatial distribution of analytes are critically important for identification and quantification of analytes.

References

1. Karas, M., Bachmann, D., Bahr, U., Hillenkamp, F.: Matrix-assisted ultra-violet-laser desorption of nonvolatile compounds. Int. J. Mass Spectrom. Ion Process **78**, 53–68 (1987)
2. Hillenkamp, F., Karas, M.:The MALDI process and method, in MALDI MS: a practical guide to instrumentation, methods, and applications; Hillenkamp, F., Peter-Katalinic, J., Eds.; Wiley-VCH: Weinheim; Chap. **1**, 1–28 (2007)
3. Walch, A., Rauser, S., Deininger, S.O., Hofler, H.: MALDI imaging mass spectrometry for direct tissue analysis: a new frontier for molecular histology. Histochem. Cell Biol. **130**, 421–434 (2008)
4. Jaskolla, T.W., Lehmann, W.D., Karas, M.: 4-chloro-α-cyanocinnamic acid is an advanced, rationally designed MALDI matrix. Proc. Natl. Acad. Sci. U. S. A. **105**, 12200–12205 (2008)
5. Costello, C.E.: Time, life … mass spectrometry—new techniques to address biological questions. Biophys. Chem. **68**, 173–188 (1997)
6. Dreisewerd, K.: The desorption process in MALDI. Chem. Rev. **103**, 395–425 (2003)
7. Garden, R.W., Sweedler, J.V.: Heterogeneity within MALDI samples as revealed by mass spectrometric imaging. Anal. Chem. **72**, 30–36 (2000)
8. Nelson, R.W., Mclean, M.A., Hutchens, T.W.: Quantitative-determination of proteins by matrix-assisted laser-desorption ionization time-of-flight mass-spectrometry. Anal. Chem. **66**, 1408–1415 (1994)
9. Bouschen, W., Spengler, B.: Artifacts of MALDI sample preparation investigated by high-resolution scanning microprobe matrix-assisted laser desorption/ionization (smaldi) imaging mass spectrometry. Int. J. Mass Spectrom. **266**, 129–137 (2007)
10. Gabriel, S.J., Pfeifer, D., Schwarzinger, C., Panne, U., Weidner, S.M.: Matrix-assisted laser desorption/ionization time-of-flight mass spectrometric imaging of synthetic polymer sample spots prepared using ionic liquid matrices. Rapid Commun. Mass Spectrom. **28**, 489–498 (2014)
11. Hu, J.-B., Chen, Y.-C., Urban, P.L.: Coffee-ring effects in laser desorption/ionization mass spectrometry. Anal. Chim. Acta **766**, 77–82 (2013)
12. Vorm, O., Roepstorff, P., Mann, M.: Improved resolution and very high sensitivity in MALDI TOF of matrix surfaces made by fast evaporation. Anal. Chem. **66**, 3281–3287 (1994)
13. Dai, Y.Q., Whittal, R.M., Li, L.: Two-layer sample preparation: a method for MALDI-MS analysis of complex peptide and protein mixtures. Anal. Chem. **71**, 1087–1091 (1999)
14. Hensel, R.R., King, R.C., Owens, K.G.: Electrospray sample preparation for improved quantitation in matrix-assisted laser desorption/ionization time-of-flight mass spectrometry. Rapid Commun. Mass Spectrom. **11**, 1785–1793 (1997)
15. Shimma, S., Takashima, Y., Hashimoto, J., Yonemori, K., Tamura, K., Hamada, A.: Alternative two-step matrix application method for imaging mass spectrometry to avoid tissue shrinkage and improve ionization efficiency. J. Mass Spectrom. **48**, 1285–1290 (2013)
16. Xiang, F., Beavis, R.C.: A method to increase contaminant tolerance in protein matrix-assisted laser-desorption ionization by the fabrication of thin protein-doped polycrystalline films. Rapid Commun. Mass Spectrom. **8**, 199–204 (1994)
17. Deegan, R.D., Bakajin, O., Dupont, T.F., Huber, G., Nagel, S.R., Witten, T.A.: Capillary flow as the cause of ring stains from dried liquid drops. Nature **389**, 827–829 (1997)
18. Hu, H., Larson, R.G.: Evaporation of a sessile droplet on a substrate. J. Phys. Chem. B **106**, 1334–1344 (2002)

19. Watrous, J.D., Alexandrov, T., Dorrestein, P.C.: The evolving field of imaging mass spectrometry and its impact on future biological research. J. Mass Spectrom. **46**, 209–222 (2011)

20. Schwartz, S.A., Reyzer, M.L., Caprioli, R.M.: Direct tissue analysis using matrix-assisted laser desorption/ionization mass spectrometry: practical aspects of sample preparation. J. Mass Spectrom. **38**, 699–708 (2003)

21. Luxembourg, S.L., McDonnell, L.A., Duursma, M.C., Guo, X.H., Heeren, R.M.A.: Effect of local matrix crystal variations in matrix-assisted ionization techniques for mass spectrometry. Anal. Chem. **75**, 2333–2341 (2003)

22. Hakomori, S.: Glycosylation defining cancer malignancy: new wine in an old bottle. Proc. Natl. Acad. Sci. U. S. A. **99**, 10231–10233 (2002)

23. Dube, D.H., Bertozzi, C.R.: Glycans in cancer and inflammation. Potential for therapeutics and diagnostics. Nat. Rev. Drug Discov. **4**, 477–488 (2005)

24. Harvey, D.J.: Analysis of carbohydrates and glycoconjugates by matrix-assisted laser desorption/ionization mass spectrometry: an update for 2007–2008. Mass Spectrom. Rev. **31**, 183–311 (2012)

25. Gabriel, S.J., Schwarzinger, C., Schwarzinger, B., Panne, U., Weidner, S.M.: Matrix segregation as the major cause for sample inhomogeneity in MALDI dried droplet spots. J. Am. Soc. Mass Spectrom. **25**, 1356–1363 (2014)

26. Mampallil, D., Eral, H.B., van den Ende, D., Mugele, F.: Control of evaporating complex fluids through electrowetting. Soft Matter **8**, 10614–10617 (2012)

27. Hu, H., Larson, R.G.: Marangoni effect reverses coffee-ring depositions. J. Phys. Chem. B **110**, 7090–7094 (2006)

28. Probstein, R.F.: Surface tension, in Physicochemical hydrodynamics: an introduction, John Wiley & Sons, Inc.: Hoboken, NJ; Chap. **10**, 305–361 (1994)

29. Majumder, M., Rendall, C.S., Eukel, J.A., Wang, J.Y.L., Behabtu, N., Pint, C.L., Liu, T.-Y., Orbaek, A.W., Mirri, F., Nam, J., Barron, A.R., Hauge, R.H., Schmid, H.K., Pasquali, M.: Overcoming the "coffee-stain" effect by compositional marangoni-flow-assisted drop-drying. J. Phys. Chem. B **116**, 6536–6542 (2012)

30. Hsiao, C.-H., Hong, C.-W., Liu, B.-H., Chen, C.W., Wu, C.-C., Wang, Y.-S.: Comprehensive molecular imaging of photolabile surface samples with synchronized dual-polarity time-of-flight mass spectrometry. Rapid Commun. Mass Spectrom. **25**, 834–842 (2011)

31. Lebedev, N.N.:Spherical harmonics: theory, and Spherical harmonics: applications, in Special functions and their applications; Prentice-Hall: Englewood Cliffs, NJ, Chaps. **7** and **8**, 161–237 (1965)

32. Deegan, R.D., Bakajin, O., Dupont, T.F., Huber, G., Nagel, S.R., Witten, T.A.: Contact line deposits in an evaporating drop. Phys. Rev. E **62**, 756–765 (2000)

33. Hu, H., Larson, R.G.: Analysis of the effects of marangoni stresses on the microflow in an evaporating sessile droplet. Langmuir **21**, 3972–3980 (2005)

34. Savino, R., Paterna, D., Favaloro, N.: Buoyancy and marangoni effects in an evaporating drop. J. Thermophys. Heat Transf. **16**, 562–574 (2002)

35. Bhardwaj, R., Fang, X., Attinger, D.: Pattern formation during the evaporation of a colloidal nanoliter drop: a numerical and experimental study. New J. Phys. **11**, 075020 (2009)

36. Ehring, H., Karas, M., Hillenkamp, F.: Role of photoionization and photochemistry in ionization processes of organic-molecules and relevance for matrix-assisted laser desorption ionization mass-spectrometry. Org. Mass Spectrom. **27**, 472–480 (1992)

37. Lai, Y.-H., Chen, B.-G., Lee, Y.T., Wang, Y.-S., Lin, S.H.: Contribution of thermal energy to initial ion production in matrix-assisted laser desorption/ionization observed with 2,4,6-trihydroxyacetophenone. Rapid Commun. Mass Spectrom. **28**, 1716–1722 (2014)

38. Lai, Y.-H., Wang, C.-C., Chen, C.W., Liu, B.-H., Lin, S.-H., Lee, Y.T., Wang, Y.-S.: Analysis of initial reactions of MALDI based on chemical properties of matrixes and excitation condition. J. Phys. Chem. B **116**, 9635–9643 (2012)

39. Liu, B.-H., Charkin, O.P., Klemenko, N.M., Chen, C.-W., Wang, Y.-S.: Initial ionization reaction in matrix-assisted laser desorption/ionization. J. Phys. Chem. B **114**, 10853–10859 (2010)

40. Weidner, S., Knappe, P., Panne, U.: MALDI-TOF imaging mass spectrometry of artifacts in "dried droplet" polymer samples. Anal. Bioanal. Chem. **401**, 127–134 (2011)

41. Shen, X., Ho, C.-M., Wong, T.-S.: Minimal size of coffee ring structure. J. Phys. Chem. B **114**, 5269–5274 (2010)